Catalysis Communications 84 (2016) 137–141

Contents lists available at ScienceDirect

Catalysis Communications

journal homepage: www.elsevier.com/locate/catcom

Promotion of $ZnSn(OH)_6$ photoactivity by constructing heterojunction with $Ag@Ag_3PO_4$ nanoparticles: Visible light elimination of single or multiple dyes

Fei Chen [a,b], Qi Yang [a,b,*], Xiaoming Li [a,b], Dongbo Wang [a,b], Yu Zhong [a,b], Jianwei Zhao [a,b], Yaocheng Deng [a,b], Chenggang Niu [a,b], Guangming Zeng [a,b]

[a] *College of Environmental Science and Engineering, Hunan University, Changsha, 410082, PR China*
[b] *Key Laboratory of Environmental Biology and Pollution Control (Hunan University), Ministry of Education, Changsha, 410082, PR China*

ARTICLE INFO

Article history:
Received 4 April 2016
Received in revised form 21 June 2016
Accepted 27 June 2016
Available online 29 June 2016

Keywords:
$Ag@Ag_3PO_4@ZSH$
Photocatalytic activity
Photoelectric property
Dye
Mechanism

ABSTRACT

In this study, novel $Ag@Ag_3PO_4$ modified $ZnSn(OH)_6$ (ZSH) photocatalyst was prepared by a facile situ deposition and photo-reduction reaction method. Superior photocatalytic activities for dye and dye mixture degradation were achieved. Moreover, preferable photoelectric performances were verified by electrochemical tests. The introduction of $Ag@Ag_3PO_4$ on ZSH and surface plasmon resonance (SPR) effect played an important role in photoelectrons transferring, photogenerated electron-holes separation and photoactivity enhancement. Simple assembling method, good reusability, high photoelectric properties and multi-component dyes wastewater treatment make it possible for practical industrial applications.

1. Introduction

In the past decades, semiconductor-based photocatalysis has attracted considerable attention attributing to its promising application in solving the worldwide energy shortage and environmental pollution using the abundant solar light [1–3]. In view of practicality, it is highly desirable to develop new-type semiconductor photocatalysts for solving problems existing in industrial productions.

To date, researchers have made unremitting efforts in exploring more easily available and high-efficient photocatalysts, such as $g\text{-}C_3N_4$ [4], Cu_2O [5], CeO_2 [6], ZnO [7], ZSH [8] and so on. The origin of ZSH for photocatalytic application should be responsible for its easy scaling up and special structure, which is full of OH groups. Restricting by the wide band energy (about 4 eV [9]), single ZSH only absorbed ultraviolet light and still fell far from satisfactory under visible light. Heterostructure fabrication to facilitate the ZSH driven photooxidation abilities under visible light seems to be reasonable, with successful cases as BiOI/ZSH [10], Ag@AgCl/ZSH [11], AgI/ZSH [12]. Besides, more adjustable semiconductors ought to be explored and to construct heterojunction structure with ZSH for sustainable development.

Most recently, the family of silver salts is found to be excited in visible light region and has displayed desirable photocatalytic performance durability [13]. As a typical silver salt, silver orthophosphate (Ag_3PO_4) exhibited a superior potential in photodegradation of organic contaminants [14]. However, some limitations were still existed in the Ag_3PO_4 photocatalytic system. One reason is that the potential of conduction band (CB) was more positive than the reduction potential of O_2 ($O_2 + e^- \rightarrow \bullet O_2^- - 0.33$ V vs NHE [15]). In turn, an important active species $\bullet O_2^-$ couldn't be formed, leading to lower photocatalytic activity. Constructing a hybrid or heterojunction structure between Ag_3PO_4 and another well-matched semiconductor was validated to be available, such as Ag_3PO_4/TiO_2 [16], $Ag_3PO_4/g\text{-}C_3N_4$ [17], Ag_3PO_4/Hap [15], Ag_3PO_4/CeO_2 [18] and so forth. Moreover, Ag_3PO_4 could be transformed into stable structure $Ag\text{-}Ag_3PO_4$ composite under illumination treatment. The forming metallic Ag not only acted as an electron acceptor, but also significantly absorbed visible light due to surface plasmon resonance effect [19]. Taken the conduction and valance band of ZSH and Ag_3PO_4 into consideration, it seems to be feasible for combining ZSH ($E_{CB} = +0.49$ eV [11]) and Ag_3PO_4 ($E_{CB} = +0.42$ eV [20]) nanoparticles.

Herein, ZSH with cubic-like structure was firstly synthesized and subsequently Ag_3PO_4 nanoparticles were deposited on the surface of ZSH, afterwards combining with photoreduction reaction to form $Ag@Ag_3PO_4$. The photocatalytic activities were evaluated by single dye and

---

[*] Corresponding author at: College of Environmental Science and Engineering, Hunan University, Changsha 410082, PR China.
E-mail addresses: feichen@hnu.edu.cn (F. Chen), yangqi@hnu.edu.cn (Q. Yang).

http://dx.doi.org/10.1016/j.catcom.2016.06.029

dye mixture degradation. The self-built heterojunction structure improved the photocatalytic performance and simultaneously strengthened the photostability.

2. Experimental

The whole details of experimental part were described in Supplementary information.

3. Results and discussion

3.1. Morphology and structure

Fig. 1 shows the XRD patterns of pure ZSH, Ag@ZSH, Ag_3PO_4@ZSH and Ag@Ag_3PO_4@ZSH. The diffraction peaks of XRD patterns belonged to standard values of cubic ZSH (JCPDS file No. 73-2384 [9]) with high crystallinity as indicated by the sharp peaks. The XRD results of Ag_3PO_4 in Ag_3PO_4@ZSH and Ag@Ag_3PO_4@ZSH curves revealed peaks at 2θ of 20.9°, 29.7°, 33.3°, 36.5°, 47.8°, 55.0° and 57.3°. The corresponding values could be indexed to be (110), (200), (210), (211), (310), (320) and (321) crystal planes of body-centered cubic Ag_3PO_4 (JCPDS file No. 06-0505 [21]). For Ag@ZSH and Ag@Ag_3PO_4@ZSH, another weak peak appearing at 40.19° ascribed to (112) plane of Ag. No other crystal phases could be detected in all patterns, suggesting that high purity was achieved in synthesis process. Moreover, the XRD patterns for the first and fourth cycle were also taken into consideration. As displayed in Fig. S1 (Supplementary information), no more discrepancy was perceived and the original crystal structure remained unchanged, indicating that high photostability of the catalyst was maintained.

The morphologies of the samples were characterized by SEM analysis, and the relevant results were displayed in Fig. S2 (Supplementary information). Uniform cubic-like morphologies with a length of 200–500 nm were vividly presented for pure ZSH (Fig. S2A). A trace amount of nanoparticles were observed in Fig. S2B, due to the generated metallic Ag. A large number of nanoparticles with the diameter of approximately 40 nm were evenly and densely decorated on the uniform structure attributing to the forming of Ag_3PO_4 (Fig. S2C) and Ag@Ag_3PO_4 (Fig. S2D) on the surface of ZSH. The decorated nanoparticles could also be distinguished on the hierarchical structures by TEM images (Fig. S2E–S2H). Furthermore, Ag@ZSH and Ag@Ag_3PO_4@ZSH were also measured by EDX analysis, as seen in Fig. S2I–S2J. The elements of Ag, O, Zn and Sn for Ag@ZSH in Fig. S2I, meanwhile the elements of Ag, O, P, Zn and Sn for Ag@Ag_3PO_4@ZSH in Fig. S2J were observed, confirming the coexistence of Ag and Ag@Ag_3PO_4 in the corresponding samples. A low-density of metallic Ag was found and the weight ratio of Ag in Ag@ZSH was about 0.0191:1, consistent with the preparation (2 wt% of metallic Ag in initial Ag@ZSH). For Ag@Ag_3PO_4@ZSH, the molar ratio of Ag/P was about 3.18:1, which was a little higher than the theoretical stoichiometric proportion of pure Ag_3PO_4, validating successful introduction of metallic Ag in the photoreduction reaction.

XPS measurements were performed to investigate the surface chemical composition and chemical states of the as-prepared samples (provided in Supplementary information). The XPS survey spectra of pure ZSH, Ag@ZSH and Ag_3PO_4@ZSH were presented in Fig. S3A, no more elements were found besides for the necessity. As shown in Fig. S3B–S3C the characteristic orbital of the Zn 2p peak and the Sn $3d_{5/2}$, Sn $3d_{3/2}$ peaks of pure ZSH, Ag@ZSH and Ag_3PO_4@ZSH were detected at peak locations at 1021.76 eV and 486.3 eV, 494.7 eV, respectively [10]. The peak at 530.9 eV (Fig. S3D) was corresponding to the orbital of O 1 s in all catalysts [22]. For Ag@Ag_3PO_4@ZSH, another signal at 133.1 eV (Fig. S3E) belonged to P 2p in the sample, due to the crystal lattice of P^{5+} in PO_4^{3-} [23]. Although there was no significant XPS signal of metallic Ag in the survey spectrum of Ag@ZSH because of its small content, the Ag 3d spectrum was also recorded (Fig. S3F). Two individual peaks at 367.8 eV and 373.9 eV were assignable to the Ag $3d_{5/2}$ and Ag $3d_{3/2}$ for Ag^0, respectively [24]. The high resolution Ag 3d spectrum for Ag@Ag_3PO_4@ZSH could be fitted to two main peaks at 366.8 eV and 373.3 eV, which corresponded to Ag $3d_{5/2}$ and Ag $3d_{3/2}$, verifying the presence of Ag^+ [25]. Two characteristic peaks for Ag^0 appeared at Ag@ZSH should be perceived over Ag@Ag_3PO_4@ZSH for same photoreduction procedure, which was in good agreement with XRD analysis.

3.2. UV–vis diffuse reflectance spectra of the samples

To investigate the optical absorption properties of as-prepared samples, UV–vis diffuse reflectance spectrum were taken into discussion. As illustrated in Fig. 2, the absorption threshold value for pure ZSH was located the wavelength of about 334 nm. On the basis of empirical formula ($Eg = 1240/\lambda$, [26] where λ is the absorption edge and Eg is the corresponding band gap), the band gap of ZSH was estimated to 3.71 eV [12], The light absorption intensity for Ag@ZSH was a little higher than that of pure ZSH. While for Ag_3PO_4@ZSH and Ag@Ag_3PO_4@ZSH, they exhibited much higher light absorption between 400 nm and 800 nm, especially for Ag@Ag_3PO_4@ZSH. The absorption region at higher wavelengths for Ag@Ag_3PO_4@ZSH represented the contribution of Ag@Ag_3PO_4 and surface plasmon resonance (SPR) effect.

3.3. Photocatalytic activity

The photocatalytic activities of ZSH, N-TiO_2, Ag@ZSH, Ag_3PO_4@ZSH and Ag@Ag_3PO_4@ZSH were evaluated by measuring the decolorization

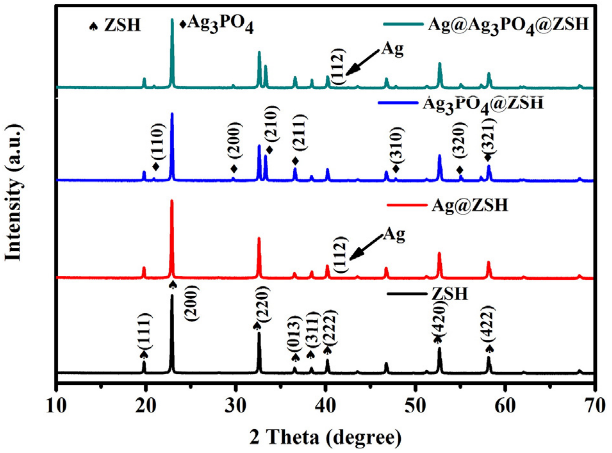

Fig. 1. The XRD patterns of pure ZSH, Ag@ZSH, Ag_3PO_4@ZSH and Ag@Ag_3PO_4@ZSH.

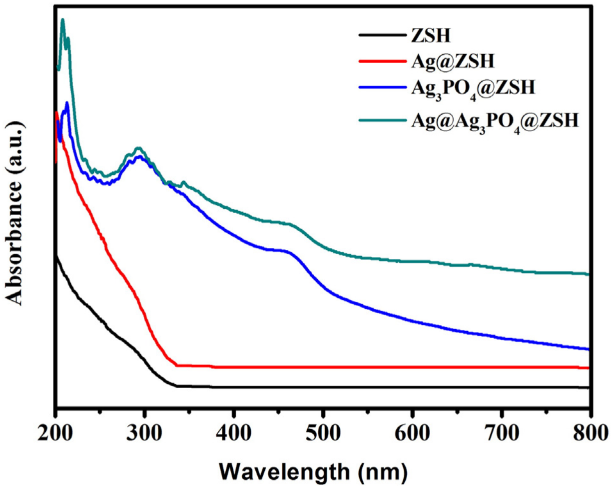

Fig. 2. UV–vis absorption spectra of the as-prepared samples.

of RhB, MO and MB under visible light irradiation. Variations of single dye concentrations (C_t/C_0) with visible-light over different photocatalysts were shown in Fig. 3a and Fig. S5a–S5b (Supplementary information). The direct photolysis and absorption of dyes were neglectable and same trends happened for RhB, MO and MB degradation. Compared with pure ZSH, Ag@ZSH exhibited a little higher photocatalytic performance. For example, only 4.3% of MO was degraded and the decomposition efficiency could reach to 19.9% by Ag@ZSH. In the presence of Ag_3PO_4, the photoactivity of pure ZSH was obviously improved. For instance RhB degradation, corresponding efficiency for Ag_3PO_4@ZSH was 88.7%, while it was 2.83% for pure ZSH. For better comparison, visible-light-driven N-TiO_2 was also fabricated, affirming the enhanced phototoactivity by Ag_3PO_4@ZSH (such as for MB degradation, 90.1% for Ag_3PO_4@ZSH and 41.2% for N-TiO_2). To highlight the advantages of Ag as an intermediate to transform electrons, Ag@Ag_3PO_4@ZSH composite was also prepared and tested the photocatalytic activity. The degradation efficiencies were 93.04%, 96.41% and 99.12% for RhB, MO and MB decomposition, respectively, higher than those for Ag_3PO_4@ZSH. The result demonstrated that the coexistence of Ag nanoparticles between Ag_3PO_4 and ZSH phases brought about more remarkable enhancement in photodegradation efficiencies. In other words, functions as an intermediate electron transfer by metallic Ag played a vital role in the photocatalytic system [17].

The discussions of FTIR spectra, dye mixture degradation and pseudo dynamics study and the reusability of Ag@Ag_3PO_4@ZSH could be found in Supplementary information.

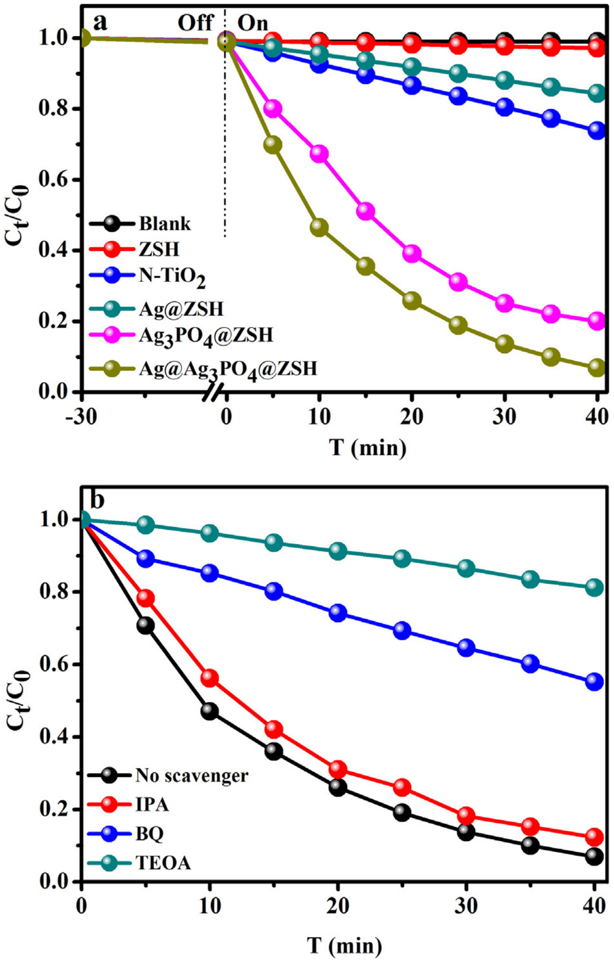

Fig. 3. Photocatalytic degradation of RhB (a) and detecting active species over RhB (b) degradation by Ag@Ag_3PO_4@ZSH.

3.4. Plausible photodegradation mechanism of Ag@Ag_3PO_4@ZSH

Detecting active species generated among photocatalytic systems is critical to understand the possible mechanism of Ag@Ag_3PO_4@ZSH system. As molecular detectors, Isopropanol (IPA, •OH quencher, 10 mM), Trietjanolamine (TEOA, h^+ quencher, 10 mM) and Benzoquinone (BQ, •O_2^- quencher, 10 mM) [11,26], were adopted to interpret the photocatalytic reactions. Cationic dye, RhB and anionic dye, MO were employed to investigate the generated active species. As displayed in Fig. 3b, Fig. S5c and Table S2 (Supplementary information), the addition of IPA induced a small reduction for dye degradation. When the scavengers of •O_2^- and h^+ were added, resulting in considerable suppression of photocatalytic activities. The photodegradation efficiencies of RhB (MO) decreased from 93.05% (96.41%) to 44.79% (43.79%) or 18.76% (21.38%) within BQ or TEOA, respectively. Thus, •O_2^- and h^+ were the most critical species while the effect of •OH could be ignored in the photocatalytic processes.

The corresponding conduction band and valence band potentials of a semiconductor can be calculated by the following equations [18,22]:

$$E_{CB} = X - E^c - 0.5E_g \quad (1)$$

$$E_{VB} = E_{CB} + E_g \quad (2)$$

where E_{CB} is the conduction band (CB) potentials, E_{VB} is the valence band (VB) potentials. X is the absolute electronegativity of the semiconductor. E^c is the energy of free electrons on the hydrogen scale (≈4.5 eV) and E_g is the band gap energy of the semiconductor. The E_{VB} and E_{CB} of ZSH were estimated to be +0.49 eV and +4.2 eV, respectively. The CB and VB energy levels of Ag_3PO_4 were calculated to be +0.45 eV and +2.9 eV, respectively [19].

PL emission was indicative for recombination of excited electrons and holes. The room temperature PL emission spectra of pure ZSH, Ag@ZSH, Ag_3PO_4@ZSH and Ag@Ag_3PO_4@ZSH were measured and illustrated in Fig. 4a. Among as-synthesized samples, Ag@Ag_3PO_4@ZSH exhibited the poorest emission intensity, indicating that electron-holes recombination processes were delayed apparently due to the introduction of Ag@Ag_3PO_4, presenting as higher photoactivity.

Photocurrent-time (PT) measurement can reflect the interfacial generation and separation dynamics of photogenerated charges of semiconductor photocatalysts [27–29]. The higher photocurrent demonstrated that higher electrons and holes separation efficiency was achieved. As depicted in Fig. 4b, in comparison with pure ZSH, Ag@ZSH and Ag_3PO_4@ZSH, Ag@Ag_3PO_4@ZSH exhibited a higher current density and verified with best photoactivity, which was in accordance with the degradation discussion.

Based on the alignments of the levels of Ag_3PO_4 and ZSH, binding with the abovementioned results, simple synthesis procedure and possible electrons transfer were illustrated in Fig. 5 and Fig. S9 (Supplementary information). Under visible light illumination, limited by the wide band gap, ZSH (3.71 eV) could not be excited by visible light and only Ag_3PO_4 (2.45 eV) was excited [15]. The photoinduced electrons of Ag_3PO_4 particles transported to the CB of Ag_3PO_4 and further flowed to the CB of ZSH, because the CB potential of Ag_3PO_4 (+0.45 eV) was more negative than that of ZSH (+0.49 eV). For Ag@Ag_3PO_4@ZSH system, metallic Ag^0 were deposited on the surface of Ag_3PO_4, leading to efficient electrons transferring. The photoinduced electrons by Ag_3PO_4 could be effectively migrated to the surface of Ag nanoparticles due to the forming good Schottky junction by contacting Ag with Ag_3PO_4. The surface plasmon resonance produced by the collective oscillations of the surface electrons induced an enhancement of the local inner electromagnetic field, resulting in desirable electron separation [22]. Moreover, the superfluous electrons on the metallic Ag^0 surface could transfer to the surface of ZSH. The accumulated electrons were trapped by dissolved oxygen to form •O_2^-, an important active species. Simultaneously, h^+ produced in the valence band of Ag_3PO_4 and generated by

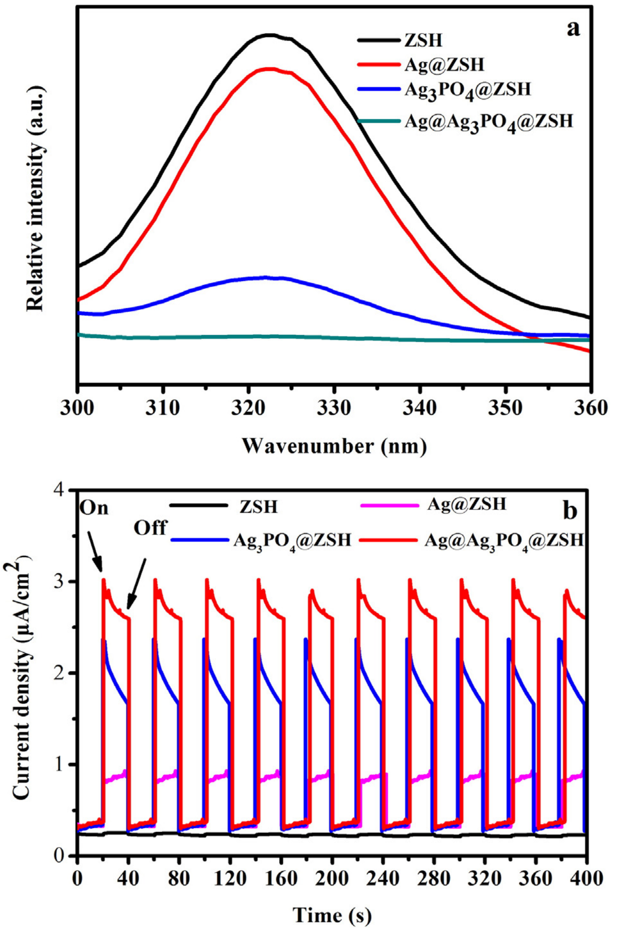

Fig. 4. Photoluminescence spectra (a) and photocurrent responses (b) of the as-prepared samples.

SPR effect degraded dye directly. In such way, the charge recombination was effectively suppressed and superior photodegradation performance was achieved. The main reactions could be listed as follows:

$$Ag_3PO_4 + h\nu \rightarrow Ag_3PO_4(h^+) + Ag_3PO_4(e^-) \quad (3)$$

$$Ag + h\nu \rightarrow Ag(e^-) + Ag(h^+) \quad (4)$$

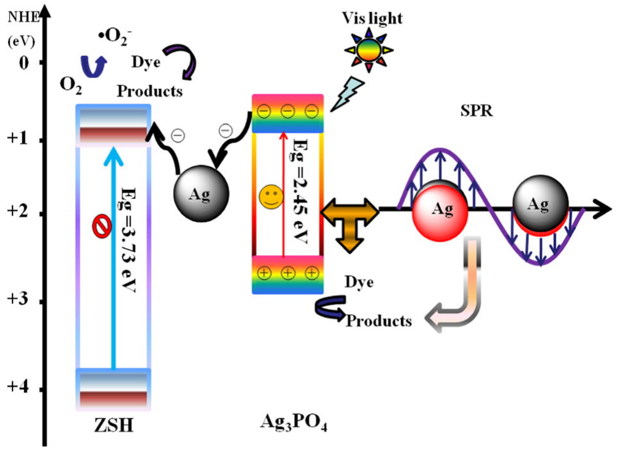

Fig. 5. Schematic diagram illustrating the proposed degradation mechanism of organic pollutants over Ag@Ag$_3$PO$_4$@ZSH composite.

$$Ag_3PO_4(e^-) + Ag \rightarrow Ag(e^-) + Ag_3PO_4 \quad (5)$$

$$Ag(e^-) + ZSH \rightarrow Ag + ZSH(e^-) \quad (6)$$

$$ZSH(e^-) + O_2 \rightarrow ZSH + \bullet O_2^- \quad (7)$$

$$\bullet O_2^- + \text{organicpollutant} \rightarrow CO_2 + H_2O \quad (8)$$

$$h^+ + \text{organicpollutant} \rightarrow CO_2 + H_2O \quad (9)$$

4. Conclusions

Novel Ag@Ag$_3$PO$_4$@ZSH photocatalyst was synthesized via a two-step approach: Ag$_3$PO$_4$ nanoparticles were firstly deposited on the surface of ZSH followed by photoreduction of metallic Ag. The photodegradation capabilities for the as-prepared samples were tested for the photocatalytic degradation of three dyes: RhB, MB and MO and their mixtures. An obvious photoactivity enhancement was acquired by Ag@Ag$_3$PO$_4$@ZSH, which was much higher than those of pure ZSH, N-TiO$_2$, Ag@ZSH and Ag$_3$PO$_4$@ZSH. Experimental investigation demonstrated that Ag nanoparticles served as carrier-transfer centers through promoting the charge transmission or separation and creating a new charge-transfer path in the photocatalytic process. The simple preparation procedure and photoelectric properties in this work may provide a new approach in the design of more novel visible-light-driven photocatalysts for practical application.

Acknowledgements

This research was financially supported by the project of National Natural Science Foundation of China (NSFC) (Nos. 51378188, 51478170, 51508178), Doctoral Fund of Ministry of Education of China (20130161120021) and Planned Science and Technology Project of Hunan Province, China (No. 2015SK20672).

Appendix A. Supplementary data

Supplementary data to this article can be found online at http://dx.doi.org/10.1016/j.catcom.2016.06.029.

References

[1] R. Asahi, T. Morikawa, T. Ohwaki, K. Aoki, Y. Taga, Science 293 (2001) 269–271.
[2] A. Kudo, Y. Miseki, Chem. Soc. Rev. 38 (2009) 253–278.
[3] R.J. Tayade, R.G. Kulkarni, R.V. Jasra, Ind. Eng. Chem. Res. 45 (15) (2006) 231–5238.
[4] J. Di, J. Xia, S. Yin, H. Xu, L. Xu, Y. Xu, J. Mater. Chem. A 2 (2014) 5340–5351.
[5] W.C. Huang, L.M. Lyu, Y.C. Yang, J. Am. Chem. Soc. 134 (2) (2011) 1261–1267.
[6] E.M. Seftel, M.C. Puscasu, M. Mertens, P. Cool, G. Carja, Appl. Catal. B Environ. 164 (2015) 251–260.
[7] A.E. Kandjani, Y.M. Sabri, M.M. Taheri, V. Bansal, S.K. Bhargava, Environ. Sci. Technol. 49 (2015) 1578–1584.
[8] X.L. Fu, X.X. Wang, Z.X. Ding, Z.Z. Zhang, J.L. Long, Appl. Catal. B Environ. 91 (2009) 67–72.
[9] Q. He, J.F. Zi, B.J. Huang, L.Y. Yan, J. Alloy Compd. 607 (2014) 193–197.
[10] H.Q. Li, Y.M. Cui, W.S. Hong, B.L. Xu, Chem. Eng. J. 228 (2013) 1110–1120.
[11] F. Chen, Q. Yang, C.G. Niu, X.M. Li, C. Zhang, RSC Adv. 5 (2015) 63152–63164.
[12] F. Chen, Q. Yang, C.G. Niu, X.M. Li, C. Zhang, Catal. Commun. 73 (2016) 1–6.
[13] Y.P. Bi, S.X. Ouyang, N. Umezawa, J.Y. Cao, J.H. Ye, J. Am. Chem. Soc. 133 (2011) 6490–6492.
[14] C.T. Dinh, T.D. Nguyen, F. Kleitzb, T.O. Do, Chem. Commun. 47 (2011) 7797–7799.
[15] Y.Y. Chai, J. Ding, L. Wang, Q.Q. Liu, J. Ren, W.L. Dai, Appl. Catal. B Environ. 179 (2015) 29–36.
[16] X.L. Ma, H.H. Li, Y.H. Wang, H. Li, B. Liu, Appl. Catal. B Environ. 158-159 (2014) 314–320.
[17] Y.M. He, L.H. Zhang, B.T. Teng, M.H. Fan, Environ. Sci. Technol. 49 (2015) 649–656.
[18] Z.M. Yang, G.F. Huang, W.Q. Huang, J. Mater. Chem. A 2 (2014) 1750–1756.
[19] J.J. Guo, H. Zhou, S.X. Ouyang, T. Kakobc, Nanoscale 6 (2014) 7303–7311.

[20] X.F. Yang, H.Y. Cui, Y. Li, J.L. Qin, R.X. Zhang, ACS Catal. 3 (2013) 363–369.
[21] H.C. Zhang, H. Huang, H. Ming, H.T. Li, J. Mater. Chem. 22 (2012) 10501.
[22] H.Y. Li, Y.J. Sun, B. Cai, S.Y. Gan, D.X. Han, Appl. Catal. B Environ. 170-171 (2015) 206–214.
[23] H. Xu, C. Wang, Y.H. Song, J.X. Zhu, Y.G. Xu, Chem. Eng. J. 241 (2014) 35–42.
[24] R.M. Mohamed, F.M. Ibrahim, J. Ind. Eng. Chem. 22 (2015) 28–33.
[25] X.X. Li, S.M. Fang, L. Ge, C.C. Han, Appl. Catal. B Environ. 176 (2015) 62–69.
[26] J. Ke, C.G. Niu, J. Zhang, G.M. Zeng, J. Mol. Catal. A Chem. 395 (2014) 276–282.
[27] D.Y. Pan, J.K. Jiao, Z. Li, Y.T. Guo, ACS Sustain. Chem. Eng. 3 (2015) 2405–2413.
[28] X.J. Bai, L. Wang, Y.F. Zhu, ACS Catal. 2 (2012) 2769–2778.
[29] F. Chen, Q. Yang, Y. Zhong, H.X. An, J.W. Zhao, Water Res. 101 (2016) 555–563.